MEASUREMENTS OF SMALL-SIZE DEBRIS WITH BACKSCATTER OF RADIO WAVES

J Markkanen, M Lehtinen, A Huuskonen, A Väänänen

Executive Summary
of
ESOC Contract No. 13945/99/D/CS
with
Sodankylä Geophysical Observatory

ESA/ESOC Technical Management
M Landgraf, R Jehn

March 2002

EUROPEAN SPACE AGENCY
CONTRACT REPORT
The work described in this report was done under ESA contract.
Responsibility for the contents resides in the authors or organizations that prepared it.

Contents

1 Overview

Our aim in this work has been to determine the feasibility of using the European ionospheric radar system EISCAT for the study of small-sized (less than 10 cm) space debris (SD). We have shown that it is technically straightforward to piggyback the SD measurements on top of the normal EISCAT ionospheric measurements, without interfering with those measurements. This could open up an extensive and efficient new radar resource for SD measurements.

The EISCAT system [1, 2, 3] consists of three separate radars: monostatic VHF radar, located near Tromsø, Norway, and operating at 224 MHz; monostatic but two-antenna EISCAT Svalbard Radar in Longyearbyen, Svalbard, operating at 500 MHz; and tristatic EISCAT UHF radar at 930 MHz, with transmitter in Tromsø and receivers in Tromsø and in Kiruna, Sweden, and Sodankylä, Finland. All the transmitters operate in the megawatt peak power range and routinely utilize high (10–20%) duty cycles.

The normal EISCAT experiment setup is not very suitable for detailed measurements of SD. The traditional EISCAT experiments operate in the "power domain" which means unnecessary neglect of phase information for signals with phase coherence time up to several hundred milliseconds. For phase coherent signals it makes good sense to add individual complex samples in such a way that they have nearly identical phase. This *coherent integration* enhances the signal with respect to the incoherent background noise. Because of the problems in the standard EISCAT experiment arrangements from the SD measurement point of view, and also because of our principle of non-interference with EISCAT operation, we have not used EISCAT digital signal processing facilities in this work. Instead, we have received the analog signal in parallel with the EISCAT receiver, with a separate receiver backend unit of our own.

The basis for our SD detection and data analysis is Bayesian statistical inversion [4]. The starting point is a parametrized model of the measurement m as $m(t) = s(t)+\gamma(t)$, where the signal s, the target echo, depends on the target range R; the Doppler-shift ω, which corresponds to the target's radial velocity; and the Doppler-drift α, which corresponds to the radial acceleration of the target. The fourth signal model parameter is the amplitude A, which depends on the target cross section, target range, and the radar parameters through the radar equation. In our model, the noise γ is parametrized by its mean power P_γ alone.

Our parameter estimates are the Bayesian estimates. These are the most probable values of the parameters, given the measurement. We have used the statistical inversion theory also to estimate the achievable parameter accuracy, mainly to compare the performance of several radars. In this work the error estimates are based on a linearised model of the measurement. The linearised model uses only he lowest-order terms of the power-series

expansion of the model signal with respect to the model parameters.

The Bayesian parameter estimation leads to a pattern matching problem. The task is to find the particular waveform, from a set of model waveforms $\{A\,\epsilon^{R,\omega,\alpha}(t)\}$, which gives the best fit to the measured noisy waveform $m(t)$. The quantity indicating the degree of match we call the *generalized match function*, GMF. For sample vectors, we define the GMF by

$$\text{GMF} \;= \left| < m, \frac{\epsilon^{R,\omega,\alpha}}{\|\epsilon^{R,\omega,\alpha}\|} > \right|, \tag{1}$$

where $< x, y >$ means the inner product of complex vectors and $\|x\|$ is the associated norm. Parameter estimation is equivalent to finding the GMF maximum. The GMF is the central tool in our analysis. If there is no noise and no acceleration, the GMF reduces essentially to what has been called the radar ambiguity function [5].

In conformity with our premise of non-interference with EISCAT operations, our approach has been to take as given whatever transmission the radar is using. We have built our data processing so that we do not need to know the transmission beforehand, instead, we measure the transmitted waveform similarly as we measure the actual signal. The measured transmission is used as starting point in the construction of the model waveforms.

The GMF-based data handling provides coherent integration of the signal. The importance of a coherent integrator as a signal detector is that its peak output is proportional to the signal energy W_s rather than just the signal power P_s. A convenient quantity, with which to measure signal detectability when coherent integration is used, is the *energy-to-noise ratio* $\mathrm{SNR_N}$, which is the ratio of signal energy to the characteristic energy scale of the noise, of temperature T_γ,

$$\mathrm{SNR_N} = W_\mathrm{s}/kT_\gamma. \tag{2}$$

This is a dimensionless quantity. For correctly sampled phase coherent signals we have

$$\mathrm{SNR_N} = N \cdot \mathrm{SNR}, \tag{3}$$

where SNR is the usual signal-to-noise ratio P_s/P_γ and N is the number of signal samples.

1.1 Study objectives

According to our contract agreement with ESOC, the objective of this study is "to define a concept how existing European radar or radio astronomy facilities can be used to detect and characterize small size debris by applying low cost hardware and software upgrades" [6].

1.2 Summary and conclusions

We focus in this study on the EISCAT incoherent scatter ionospheric radars, located in northern Scandinavia and on Svalbard. We show performance estimates which indicate that the EISCAT UHF (930 MHz) radar is the most sensitive and accurate of the EISCAT radars for SD work. The expected performance is the same as the German TIRA radar's.

We apply Bayesian statistical inversion to the SD measurement problem. We start from a four-parameter model (amplitude, target range, velocity, acceleration) of the SD signal and find a probabilistic solution for the parameters, given the sampled noisy signal m. The parameter estimation amounts to maximization of a quantity we call the Generalized Match Function, GMF [see Eq. (1)]. The GMF method automatically makes use of signal coherence to enhance detection sensitivity. Also, very little needs to be known about what the host radar is doing, the full information we can gain from he measurement is contained in m and $\epsilon^{0,0,0}$. We develop the GMF formalism from first principles in the Final Report of this study [7].

For the SD measurement we want coherent integration, which EISCAT neither needs nor provides for. To allow atmospheric and space debris measurements to proceed simultaneously, we use a separate receiver backend of our own in parallel with the EISCAT receiver. The SD receiver has a two-channel sampler, a memory buffer, and programmable control. The samples flow to the buffer which is visible to a workstation. The workstation stores the data to disk at the sampling rate, 2–3 Msamples/s. In this study, we analysed our data off-line; the final aim is real-time detection. We estimate that real-time detection in the GMF scheme requires at least 1 Gflop/s computing speed. We have developed the necessary programs to scan, archive and analyse off-line the large amounts of data, 20–30 GB/h, that our approach produces. We describe the main features of this software.

Analysis of our February 2001 test campaign at EISCAT UHF radar allows the following observations.

- We get 10–15 events per hour.
- Most events are seen in the altitude band 800–1200 km.
- The detection limit is 2 cm at 1000 km range, with 1 MW transmission peak power and 0.3 s coherent integration.
- Range can be determined essentially with the accuracy corresponding to the gate separation, about 0.1 km.
- Doppler-velocity can be determined with about 0.1 km s^{-1} accuracy or better in most cases.
- It has not been possible to get a good estimate for acceleration, but the circular-orbit value is good enough for the detection purposes as long as almost vertical antenna pointing is used.

We also compared our strongest event with catalogue predictions, and found

a reasonable agreement.

The test campaign showed that using the SD receiver, the SD measurements can proceed in the background of standard EISCAT ionospheric measurements. There are a few things that need to be taken care of before routine operations could begin.

- We need real-time detection capability. This requires that key parts of our MATLAB-based software is coded with a compiled language. We also need an environment which allows distributing the detection computations among a few networked workstation on scan-by-scan basis.
- We need to streamline our data analysis, to make it more automated. We need to include valid error estimates into our event parameter listings.
- We need to analyse the data further, to extract orbital elements based on circular-orbit approximation, and to provide error estimates for them.

In the longer term, we should not forget the unique tristatic property of EISCAT UHF system, which allows the determination of true orbit and true scattering cross section from a single measurement, without any additional assumptions. However, tristatic SD measurements, as well as all other changes in EISCAT standard experiments, require EISCAT's active participation, and are therefore at odds with the low-profile, no-interference approach that we have adopted in this study.

We have shown that there are no technical nor operational reasons why EISCAT could not help substantially in space debris monitoring, perhaps on the level of several thousand analysed events per year. This can happen without causing any interference with EISCAT's primary ionospheric mission, and with minimal extra cost.

2 Theory

2.1 Analysis by the radar equation

We used the radar equation and the Rayleigh formula for the radar cross section of a conducting sphere to compare the sensitivity of the EISCAT radars, as well as a few others. We have computed into Table 1 a "reference diameter". We assume that all the radars are capable of coherent integration, and define the reference diameter as the diameter of the conducting sphere which makes the energy-to-noise ratio $\mathrm{SNR_N}$, Eq. (2), equal to unity from 1000 km range, with 0.1 s coherent integration.

Table 1 lists three EISCAT radars and three other radars, included for comparison. The non-EISCAT radars are the TIRA tracking radar of Forschungsgesellschaft für Angewandte Naturwissenschaften (FGAN) at Wachtberg in Germany, a new weather radar of the Finnish Meteorological Institute at Luosto (LUO) in Finland, and a hypothetical radar which we call the U5G. The U5G radar combines the 32 m antenna of the EISCAT UHF system at Sodankylä with a 3 kW transmitter to operate at about 5 GHz.

Table 1: Radar properties and the reference diameter

Radar properties:	VHF	ESR	UHF	TIRA	U5G	LUO
Frequency [MHz]	224	500	933	1330	5000	5625
Wavelength [m]	1.338	0.600	0.321	0.225	0.060	0.053
Transmission [MW]	3.0	1.0	1.5	1.6	0.003	0.3
Antenna gain [dB]	43.1	45.3	48.1	49.7	62.5	47.5
Max duty cycle [%]	12.5	25.0	12.5	3.7	25.0	0.12
Noise temperature [K]	100	60	80	209	60	300
Reference size:						
Ref. diameter [cm]	2.47	1.57	1.13	1.27	(0.51)	12.7

The result of this comparison is that the EISCAT UHF and the FGAN TIRA radars are about equally sensitive, and are the most sensitive of the existing radars. It appears that the suggested U5G system, which combines a high frequency, low power transmitter with a large antenna, would be by far the most sensitive system.

2.2 Statistical inversion

We assume that the SD target has constant radial acceleration during the time it passes the radar beam. Then we can we model the measurement as

$$m(t) = s(t) + \gamma(t), \tag{4}$$

where $\gamma(t)$ is noise with power σ^2, and the signal $s(t)$ is a scaled, Doppler-shifted and delayed replica of the transmission $\epsilon^{\mathrm{T}}(\mathrm{t})$,

$$s = A\,\epsilon^{R,\omega,\alpha}(t) = A \cdot \epsilon^{\mathrm{T}}(t - \frac{2R}{c})e^{i\omega t}e^{i\alpha t^2}. \tag{5}$$

The last factor, quadratic in time in the exponent, comes from the acceleration. We note that s depends linearly on the amplitude and non-linearly from the other parameters R, ω, α.

Given a measurement m, what can we infer about the parameters A, R, ω and α? The Bayesian statistical inversion theory states that the most we can know is the *posteriori density* $D_{\mathrm{p}}(A, R, \omega, \alpha|m)$. It is the conditional probability density of the signal actually having parameters A, R, ω and α, given the measurement m, and possibly some external, *a priori* information. The theory gives means for computing the four-variable function D_{p}, for each measurement m. We use as the parameter estimates those values which maximize the posteriori density for the given measurement.

In the Final Report we show that the parameter estimation reduces to maximizing the generalized match function GMF.

- The location of the GMF maximum gives the estimates $\widehat{R}$, $\widehat{\omega}$, and $\widehat{\alpha}$,

$$(\widehat{R}, \widehat{\omega}, \widehat{\alpha}) = \arg\max_{R,\omega,\alpha} \mathrm{GMF}. \tag{6}$$

- The value of the GMF maximum gives the energy-to-noise ratio $\mathrm{SNR_N}$,

$$\widehat{\mathrm{SNR_N}} = \mathrm{SNR_N}(\widehat{R}, \widehat{\omega}, \widehat{\alpha}) = [\mathrm{GMF}(\widehat{R}, \widehat{\omega}, \widehat{\alpha})]^2/\sigma^2. \tag{7}$$

Target detection is done by comparing $\widehat{\mathrm{SNR_N}}$ against a fixed threshold. In practise we do the detection in two phases, using as an intermediate a quantity we call the *ratio*, $\mathcal{R}$, which has the property $\mathcal{R}_{\max} = \sqrt{\widehat{\mathrm{SNR_N}}}$.

- First maximize GMF/σ with respect to velocity and acceleration, to get the convenient-to-plot and economic-to-store function $\mathcal{R}(R)$,

$$\mathcal{R}(R) = \max_{\omega,\alpha} \sqrt{\mathrm{SNR_N}(R, \omega, \alpha)}. \tag{8}$$

- Then find $\mathcal{R}_{\max} = \max_R \mathcal{R}$, and check if it exceeds detection threshold,

$$\text{Detection} \longleftrightarrow \mathcal{R}_{\max} > \text{ Threshold}. \tag{9}$$

2.3 Error analysis in a linearised model

The model signal (5) can be linearised by expanding it into power series with respect to the model parameters, and taking the leading terms. Statistical inversion theory then gives analytic expressions for computing the parameter error estimates, the diagonal elements of the covariance matrix.

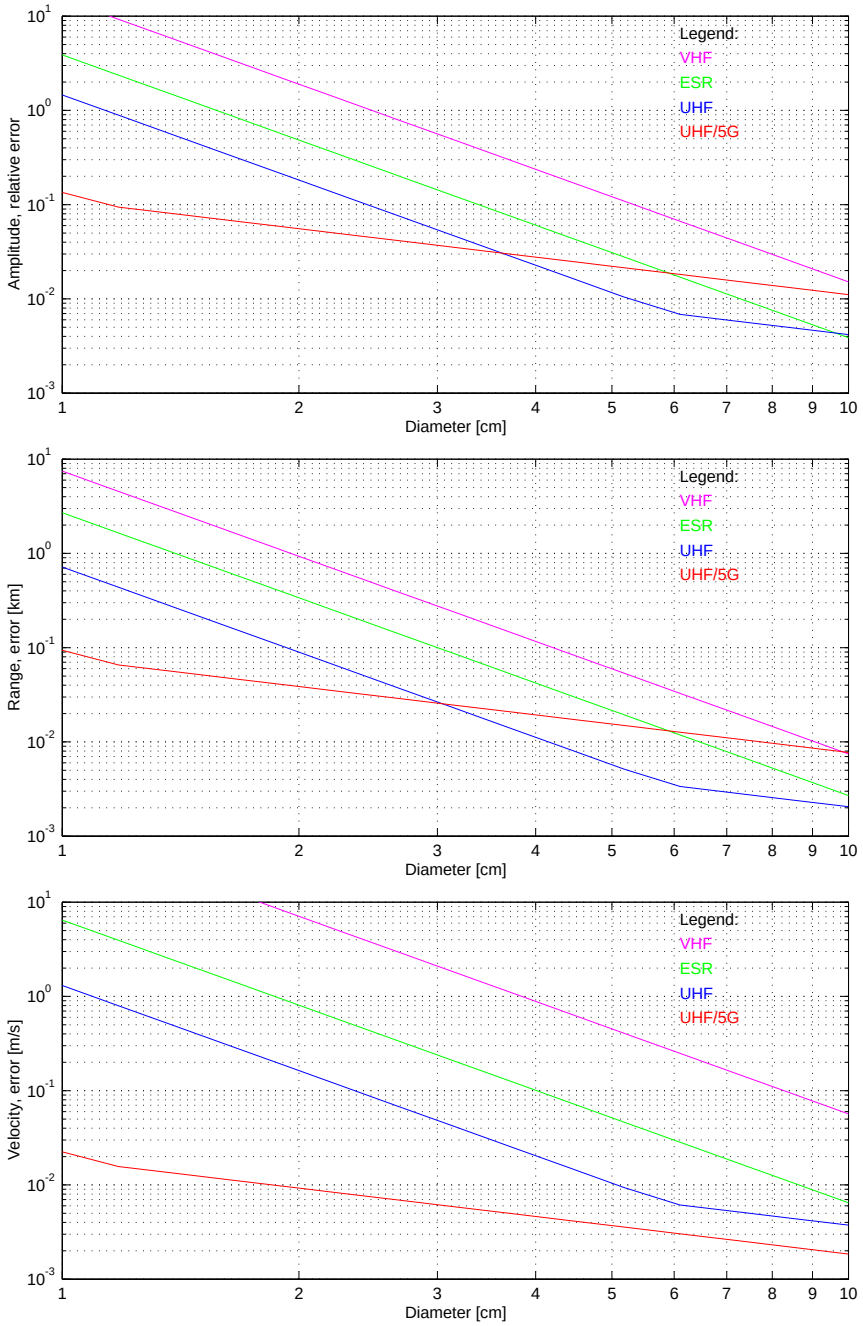

Figure 1: Relative error of signal amplitude and absolute error of target range and velocity as a function of target diameter for the EISCAT radars. We assume a spherical target at 1000 km range and assume 0.1 s coherent integration. The error curves are based on the linearised measurement model.

Figure 1 shows the 1-σ error of the model parameters as function of the diameter of the spherical target. The UHF radar is the most accurate of the EISCAT radars, as expected from the sensitivity comparison. However, the validity regime of the linearised theory, and hence the quantitative significance of the error curves, is not clear.

2.4 Computational aspects

To find the GMF maximum and get the signal parameters, we discretize the parameter space into uniform, finite $(R_j, \omega_k, \alpha_l)$-grid, and perform an exhaustive search over the grid. The range is discretized by the sampling, to typical resolution of about 100 m. The frequency discretization is determined by the length of the coherent integration, and typically corresponds to velocity step of about 1 m s^{-1}. Acceleration step that is compatible with the velocity step is a few m s^{-2}.

An example of a two-dimensional GMF (we ignore acceleration) is shown in Fig. 2, plotted on velocity-range plain. The data is from a pre-contract test campaign at ESR, where the EISCAT experiment was so called tau0 experiment. The data has high SNR, thus the figure serves to illustrate the form of the GMF in the absence of noise. The GMF oscillates wildly both in range and in velocity direction.

The computation of the discretized GMF, GMF$(R_j, \omega_k, \alpha_l)$, makes use of FFT. For each range gate j and acceleration parameter l, the GMF is computed for all Doppler-shifts k by a single M-point FFT, where M is the number of samples used in the integration.

Even with FFT, the computation task involved in SD detection, with full range and time resolution, and without any further approximations, is overwhelming. Assume we need to cover 1000 km in range and use 0.3 s integration. Assume that the sampling interval is 0.5 μs. Then $M = 600\,000$, and the FFT requires about 60 Mflops. The $1000/0.075 = 13\,000$ range gates require about 800 Gflops. If we also want to cover, say, a ± 20 m s^{-2} interval of acceleration values around a range-dependent first-guess value, with grid spacing 3.5 m s^{-2}, we need about 8 Tflops. From a workstation one can expect about 1 Gflop/s computing speed, so we would need about 8000 s to handle the 0.3 s of data, or three years to handle one hour.

However, it is possible to make several approximations, so that the prospects for real-time detection by affordable means are fairly good. The computation speed required for real-time detection depends

- on the GMF algorithm,
- on the length of integration, which together with the sampling interval determines the input data size M,
- on the number of range gates to handle,
- on the number of acceleration values to use, and

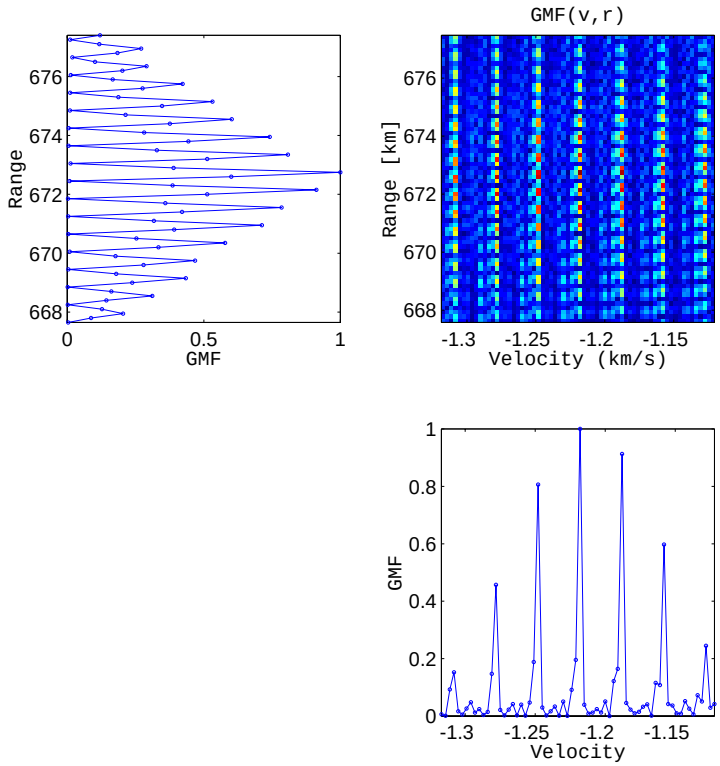

Figure 2: Measured generalized match function. The data are from a pre-contract test campaign at ESR in November 1999. The standard experiment tau0 was used for transmission. The figure shows the region around the maximum position of the GMF. The surface GMF(v, R) is shown in the top-right panel as a colour-coded image, while the other two panels show cuts of the surface through its maximum position.

- ▷ on how soon after a search scan we make the next scan.

We now comment on each of the these items.

GMF algorithm

The radar duty cycle in EISCAT experiments is about 10% in the UHF and about 20% at ESR. Therefore, in the GMF computation the FFT is done on a vector that has 80–90% of its length zeros, in regularly placed blocks. Also, the 10–20 kHz bandwidth needed to cover the SD signal is narrow compared to our sampling frequency of a few MHz. This means that not much information will be lost if we re-sample our data with reduced rate. At the price of of some loss of accuracy and sensitivity, it is possible to reduce the number of arithmetic operations drastically, typically by a factor of about one hundred. We call the resulting method of fast but approximate

GMF evaluation the FastGMF algorithm.

Both simulations and results of the test campaign show that one loses on the average only about 10% of sensitivity if one uses FastGMF instead of the standard GMF.

Length of integration

It appears that in practise it does not help much to increase integration beyond about 0.3 s. This is illustrated in Fig. 3. It is not clear why we do not gain—and can even lose—from increased integration. The signal model, rather than our software, seems to be failing, for we do get the expected $\mathcal{R}_{\max} \propto \sqrt{N}$ behaviour when we feed simulated data to the analysis program.

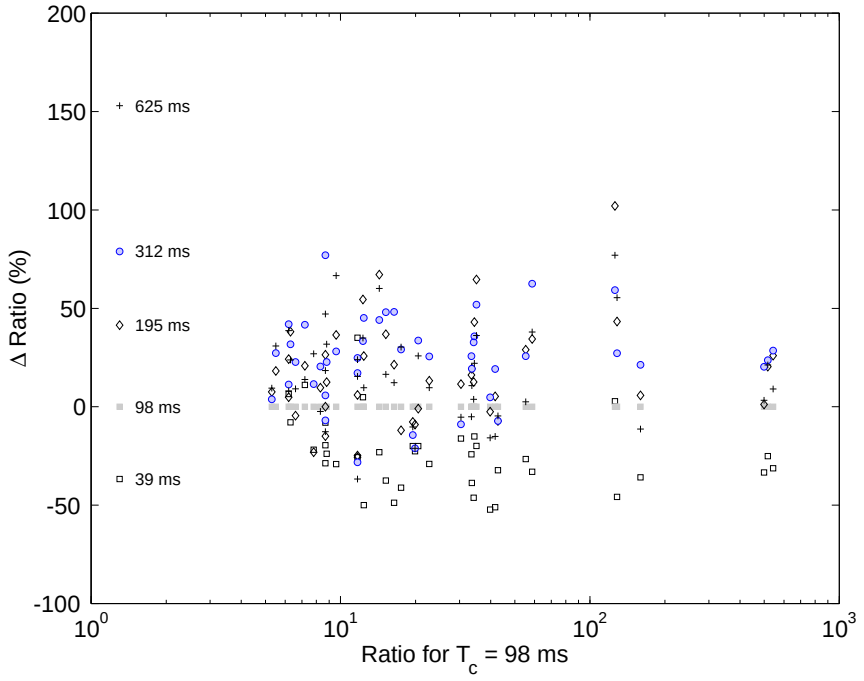

Figure 3: Dependence of $\mathcal{R}_{\max}$ on integration time. A fixed data set from the test campaign was analysed with five different integration times T_{c}. The ratio $\mathcal{R}^{T}_{\max}$ is compared with the reference ratio, $\mathcal{R}^{98}_{\max}$. The markers in the left indicate the expected difference $\Delta\mathcal{R}_{\max}$ if the coherent integration would be fully successful. X-axis is $\mathcal{R}^{98}_{\max}$, Y-axis is $(\mathcal{R}^{T}_{\max} - \mathcal{R}^{98}_{\max})/\mathcal{R}^{98}_{\max}$.

Range grid and range coverage

The test campaign showed that in practice we can cover about 1000 km in range, say from 500 km to 1500 km, with a 100–200 km gap somewhere

inside (see Fig. 7).

The required range gate spacing depends on the transmission. If there is only a single frequency in the transmission, the GMF in the range direction is a smoothly varying function, the code autocorrelation function, centred near the actual target range. With multiple frequencies—which almost always is the case in EISCAT—on top of this smooth variation, the GMF exhibits a much faster oscillation in the range direction, as shown in Fig. 2. However, it turns out that the relevant scale even in the multi-frequency case is the code baud length, not the period of the faster oscillation, and it suffices to use range grid spacing that is some sizable fraction x of the code baud length. For example, when we analysed test campaign data with $x = 0.46$, in 90% of events we lost less than 27% of $\mathcal{R}_{\max}$ in comparison to the same data analysed with the maximal range resolution, $x = 0.03$

Acceleration grid

Selecting the acceleration grid for detection has turned out to be very simple: no grid is needed. A single, range-dependent value is good enough as long as the antenna is pointed nearly vertically. The value we have used is computed assuming that the target is in circular orbit. Both simulations and the data from the test campaign indicate that not much sensitivity is lost in practice even if the acceleration is not varied. Even without any acceleration correction ($\alpha = 0$), the mean reduction in $\mathcal{R}_{\max}$ among 45 test campaign events was only 33%.

Real-time computing requirement

If we further assume that it is sufficient to sample with 2 MHz rate, and accept that with 0.3 s integration it is possible to tolerate 0.2 s blank time between successive integrations, we can determine the number of flops per seconds needed to handle the detection in real time. This we have done in Table 2.

Our detection and analysis software has been programmed using the MATLAB™ high level programming language and programming environment. MATLAB itself is an interpreted environment, but it allows user-defined, compiled c-language extensions. The GMF evaluation has been implemented as such an extension. We used MATLAB's flops counter to get the number of arithmetic operations needed for a single range gate in the FastGMF algorithm. This number is shown in the second line of Table 2 for three experiments. Taking also the non-FFT operations into account, the cp1lt experiment requires 0.71 Mflops per range gate.

We also do acceleration correction here, though we only handle one acceleration value per gate. In cp1lt we need 740 range gates, to cover 1000 km with 1.35 km (9 μs) resolution. This requires 525 Mflops. To perform two

Table 2: SD detection computing power requirements in some EISCAT experiments, in the FastGMF algorithm.

	cp1lt	tau2	tau0
Sampling rate (μs)	0.5	0.5	1.0
Mflops in FFT/gate	0.27	0.27	0.27
Total Mflops/gate	0.71	0.80	0.83
Baud length (μs)	21	36	64
Range resolution (μs)	9	10	15
Number of gates/scan	740	666	444
Number of gates/s	1480	1330	890
Req. computing rate (Gflops/s)	1.1	1.1	0.7

scans per second thus requires about 1.1 Gflops. We get a similar speed requirement for tau2. Tau0, for ESR, is easier, basically because of the lower frequency that is used there.

We estimate that four G4-level power-PCs should be able to handle detection in real time, when the algorithms are carefully coded in a compiled language.

3 Measuring System

3.1 Hardware

EISCAT UHF radar

Main blocks of the EISCAT UHF radar are shown in Fig. 4. The receiver has a cooled preamplifier, which receives the radio-frequency (RF) signal around 929 MHz from the antenna thought a duplexer-polarizer system. The RF signal is converted to first intermediate frequency (IF1) around 117 MHz, and then to the second intermediate frequency (IF2) around 11 MHz. The analog signal path is bandlimited to 7 MHz width by a filter centred at 11.25 MHz. The second IF is digitized by a 14-bit A/D converter, using 15 MHz sampling rate, and distributed to the multichannel EISCAT digital receiver.

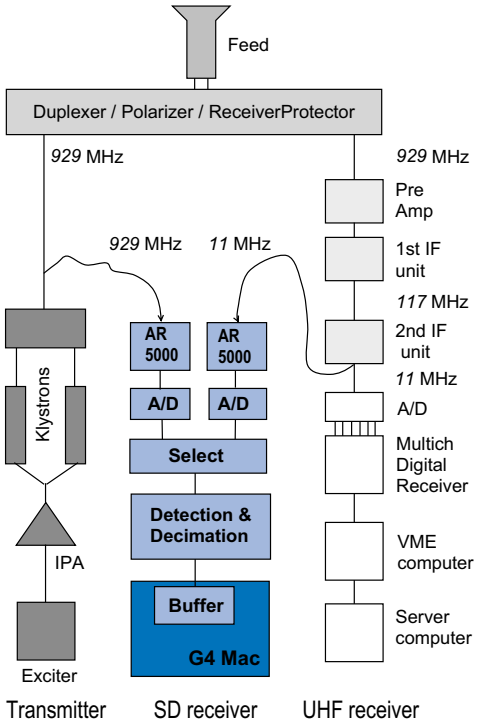

Figure 4: EISCAT Tromsø UHF radar and our SD receiver.

The EISCAT UHF transmitter consists of a programmable radar controller that generates the pulse patterns at DC level, either uncoded on/off "long pulses" or various classes of binary phase codes; an exciter system that converts the radar controller output to RF; and a klystron power amplifier which consists of two klystron tubes, delivering combined peak power of about 2.5 MW. The maximum power that can actually be transmitted is

limited by the waveguide system to a value that is somewhat below 2 MW, however. The maximum transmitter duty cycle is 12.5%, and duty cycles near this value are also used in practice.

The 32 m UHF antenna is fully steerable parabolic dish, has Cassegrain optics, and has a rotation rate of about 80°/min both in azimuth and elevation.

The time and frequency base at all EISCAT sites is from the GPS system.

The space debris receiver

To be able to measure in parallel with EISCAT, an additional data collecting system is needed. Coherent integration requires that the raw samples are available, so an independent system from the analog level onwards is needed. The SD receiver can hook on any analog frequency, and as a matter of principle, we would prefer to take the signal as near the antenna (as unprocessed) as possible. For the February 2001 test campaign in Tromsø, we used the EISCAT second IF as the analog input. Figure 4 shows the main blocks of the SD receiver and its connections to the EISCAT UHF system.

EISCAT experiments normally use more than one frequency. EISCAT itself handles this situation in the traditional way, by having multiple hardware channels, each tuned to a particular frequency.[1] The end result is several sample streams, one for each channel. Our approach in the SD receiver is different. We sample fast enough to capture the whole relevant analog band into a single digital stream. If the spread of frequencies is B MHz, we take slightly more than B million complex samples per second. The largest frequency spread during the test campaign was 2.1 MHz. It was handled by taking 2.5 million complex samples per second.

In addition to sampling the target echo, we also need to sample during the transmission periods, to get the code patterns. At its ESR site, EISCAT provides the transmission sample signal on the same data path as the reception, so no special arrangements are needed there. In Tromsø, this service is planned but was not available during the test campaign, so we had to resort to ad hoc arrangements. We sampled the transmission with the same sampling rate as the reception.

Our data acquisition system has originally been developed for ionospheric tomography by a Finnish company, Invers Ltd. The basic system consists of a sampling section, a demodulation and decimation section, and a computer interface section which has a large data buffer and a control interface. The system supports three analog input channels. We used two channels, one for transmission sampling, the other for reception sampling. The transmission channel was level-detected, and when found active, was selected as the data source. For all other times, the receiver channel was used as the data source.

[1] Under experiment program control, the tuning can be changed in microsecond time scale.

The raw sampling rate was 40 MHz. The resulting real-valued sample stream was processed by programmable logic circuitry to perform demodulation, essentially by doing Hilbert transform as follows. If the 40 MHz stream has samples x_1,$x_2 \ldots$, the first complex sample is $z_1 = (x_1, x_2)$, the next complex sample is $z_2 = (x_5, x_6)$, and so on. The stream of the z_n-samples thus has sampling interval 100 ns. For narrowband analog input around 10 MHz, the z_n-sequence represents the positive-frequency part of the double-sided analog spectrum.

The complex 10 MHz sample stream is decimated as required and written to the output buffer. The decimation is done by adding an appropriate number of consecutive complex samples, thus ensuring proper filtering.

The output buffer and the control circuitry are mounted on a PCI slot of a fast workstation. We are using Mac G4 workstations, running under the Mac OS X version of UNIX. Software from the Invers Ltd is used to read the data from the buffer and write them to hard disks. Typical data accumulation rate is between 20-30 Gbytes/hour. For long-term storage, data are copied to 60–70 GByte FireWire disks.

3.2 Software

Figure 5 shows a conceptual block diagram of our SD software, as it would be used in real-time operation. All the main tasks were implemented already for the test campaign, but the software was operated off-line, using data recorded on disks. In real-time operation, only a large buffer of raw data would be kept on disk. Whether real-time or off-line, conceptually we view the data as a continuous stream.

The software to process the data stream is a chain of four modules: the scanner, the detector, the archiver and the analyser. For this study, we have implemented the processing chain as two MATLAB programs, SPDSCAN and SPDVIEW.

Data stream

The digital SD data stream consists of primary data and auxiliary data. The primary data, produced by the SD receiver under the control of the GURSIP^{TM} software of Invers Ltd, consists of 32-bit words. Of a word, 15+15 bits are used by a complex integer which represents a measured sample, either a transmission sample or a reception sample. The remaining two bits contain two flags. One flag tells whether the data sample is a transmission sample or a reception sample. The other flag is a GPS-based full-second time mark, accurate to a few μs.

The auxiliary data consist of a time stamp and radar state information. The GURSIP software inserts a fully qualified time stamp, based on the recording computer's timekeeping, into a log file at the start of the

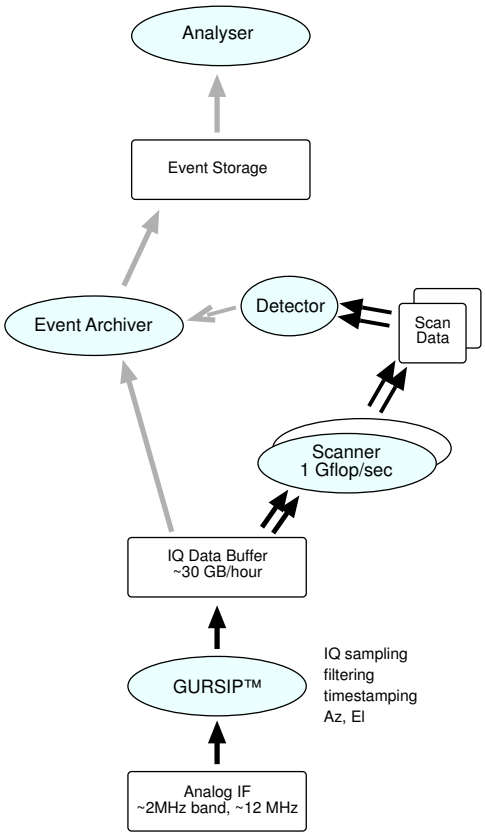

Figure 5: Main software modules for SD measurement.

recording. Starting from the time stamp and counting the samples in the continuous sample stream, we are able to get the actual UT time of any data segment with about 10 ms accuracy, mainly limited by the accuracy of the workstation clock. For routine SD measurements, antenna pointing direction should be recorded. In EISCAT, these data are only available via the radar process computer. We would need EISCAT to provide a server program capable of returning the azimuth and elevation when queried. It is useful to have the transmission power included into the data stream also, although we can monitor the relative changes of the power via the transmission samples. Neither the antenna position nor the transmission power were available on-line during the test campaign. On the other hand, only fixed antenna pointing was used, so we could easily keep track of the pointing direction during data analysis .

Scanner

The most time consuming task of the data processing, GMF computation, is done by the program SPDSCAN. For real time detection, it might become

necessary to run the scanner on several networked computers. The scanning task is straightforward to parallelise on scan-by-scan basis, so we do not expect the parallelisation to present a big problem in practice. Parallelisation on this level, including the distribution of the tasks and collecting the results, is a standard feature of the GURSIP software. The files produced by SPDSCAN are used as the input by the detection, archiving and analysis program, SPDVIEW.

Target detection and initial parameter estimates

Before actually attempting detection, it is possible to use SPDVIEW to inspect interactively the ratio profiles produced by SPDSCAN. It is also possible to "clean" the profiles. Detection is done on the cleaned data.

When the detection threshold is exceeded, SPDVIEW computes initial estimates for target range, Doppler velocity and the signal-to-noise ratio. If also the acceleration has actually been determined by the scanner, by varying the acceleration parameter in the GMF, also the acceleration is returned. However, in almost all cases, we have fixed the acceleration to the circular-orbit value.

The initial parameter estimates obtained as side product of detection are deduced directly from the profiles collected by the scanner, with the particular range, time and spectral resolution used by the scanner. The preliminary values are used to group the individual scans into events, corresponding to a single target when it moves though the radar beam. SPDVIEW provides automatically a preliminary grouping, based on finding a detectable spike in the $\mathcal{R}$ profiles at nearly the same range in nearby scans. The grouping can be improved by interactive inspection.

Event archiver

After an event has been identified, SPDVIEW is used as a rudimentary archiver to save the raw data and the auxiliary information to an event-specific directory. The amount of raw data to be archived is large but not unmanageably large. In the test campaign, about 15 events per hour were found. To store 10 seconds of raw data around each event would amount to storing 150 seconds/hour. Assuming 2 Msamples/s sampling rate and four-byte complex samples, 150 seconds/hour corresponds to about 900 measuring hours per terabyte of available storage, if all ranges are kept. As the largest available tape units and FireWire disks presently take about 100 Gbytes of data, storing one year's measurements as uncompressed raw echoes would require about 10 or a dozen such tapes or disks. This seems a quite reasonable cost. A planned FFT-based data compression algorithm, for storing only the necessary limited frequency bands, could result in a further compression by a factor of about 5 in the average. Storing only limited range intervals

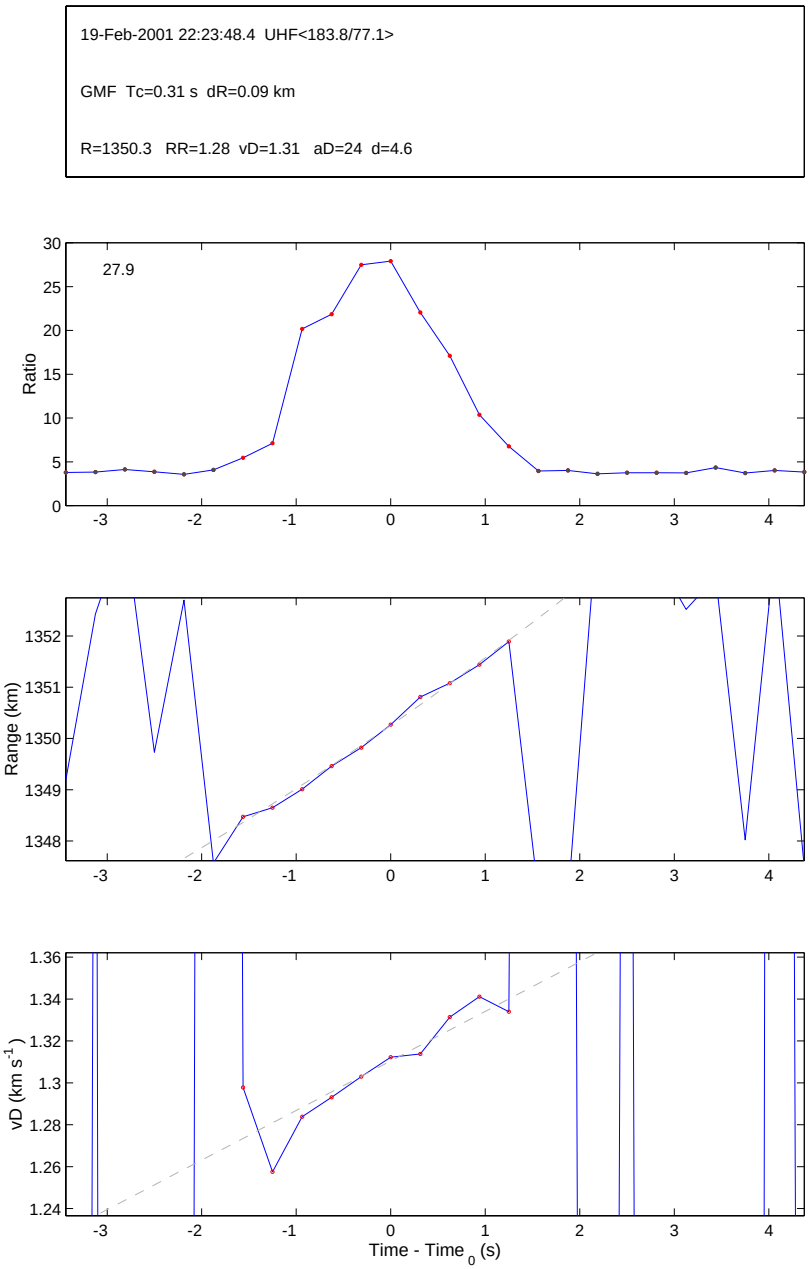

Figure 6: Event summary plot for an event in experiment cp1lt, 19 February 2001. The event was analysed with the standard GMF algorithm. The header panel shows the deduced event parameters, which include time of maximum signal strength, and, for that instant of time, target range, range-rate as fitted from range data, Doppler-velocity, and minimum diameter.

in an experiment which has 12.5% radar duty cycle, would reduce the storage needs by a further factor of 8. If both compression modes are used, the required storage space for one year's measurements goes down to about 25–30 Gbytes.

Analysis

The scanner acquires initial estimates of target range and velocity as side product of the detection, but the final determination of the target parameters is done separately with SPDVIEW, using raw data from the event archive. The analysis consists of two phases. First the event's raw data are re-scanned with full time and range resolution, optionally using the full GMF algorithm. This becomes possible because after detection, we can restrict to a few kilometers the range where the GMF is evaluated. In the second phase, we plot the parameters from individual scans as function of time, and, when possible, fit low-order polynomials to the range and velocity data. Figure 6 is an example of such an event summary plot.

4 Test Measurements

4.1 Test campaign

Our contract stipulates a series of test measurements to be performed and analysed. We did the measurements at the EISCAT UHF radar during a Finnish EISCAT measuring campaign which lasted from 11 February to 23 February 2001, using the SD receiver as shown in Fig. 4.

Two standard EISCAT experiments were in use during the campaign, the cp1lt experiment and the tau2 experiment. We took 16.5 hours of cp1lt data, with sampling rates from 2.5 MHz to 1.1 MHz, and 1.7 hours of tau2 data, with 2 MHz sampling. This gave about 0.5 TBytes of data which were stored on 13 FireWire disks. We have analysed 2.8 hours of cp1lt and 1.2 hours of tau2 data.

4.2 Analysis results

Detection rate and altitude coverage

There were 45 (cp1lt) + 11 (tau2) clear hard target events in the 4 hours of analysed data. "Clear" here means that the event had more than one scan exceeding the detection threshold, and that the deduced target parameters were sensibly located in the range-velocity space from scan to scan. The mean event rate was 13 events per hour. The combined SD search region in the two experiments was from 400 km to 1750 km in altitude. Figure 7 shows the altitude distribution of the events and also indicates the "blind zone" of each experiment. The blind zone is an altitude interval from which no target echoes can be received, due to ongoing transmission. The tau2 blind zone is in the middle of the highest event density in cp1lt. This might partially explain the somewhat lower event rate in tau2, nine events per hour, compared to 16 events per hour in cp1lt.

Detection sensitivity and effective diameter

After experimentation with various values, $\mathcal{R}_{\max} = 5$ was used throughout as the detection threshold. One cannot use much lower threshold than 5, for example, already threshold 4 gives a false alarm in almost every scan that goes through the full altitude range.

Given the length of integration, duty cycle, system temperature, transmission power and target range, $\mathcal{R}_{\max}$ can be converted to effective target diameter with the help of the radar equation. Figure 8 shows the minimum detectable diameter as function of range for the cp1lt and tau2 experiments. For example, at 1000 km range, $\mathcal{R}_{\max} = 5$ corresponds to 2.1 cm diameter in cp1lt and 1.9 cm in tau2. The greater sensitivity of tau2 is due to the higher duty cycle, 8.8% in tau2 contrary to 7.0% in cp1lt. The assumed

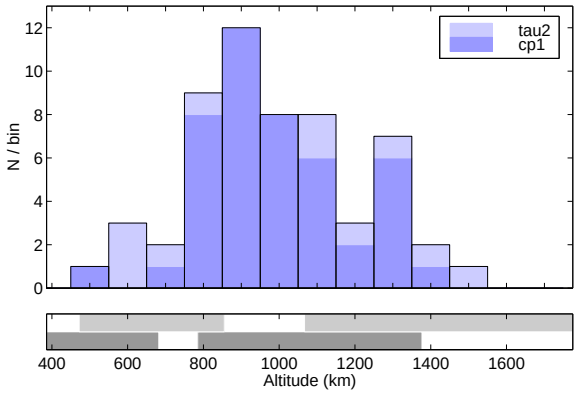

Figure 7: Altitude distribution of events in the test campaign, February 2001. The cp1lt data are from 19 February, 22:23–01:11 UT (45 events), the tau2 data are from 20 February, 21:26–22:40 UT (11 events). The main panel shows the altitude distribution of all the 56 events, the bottom panel indicates the SD search bands in the two experiments. In tau2, the first blind zone is in 855–1067 km, in cp1lt, in 682–785 km altitude.

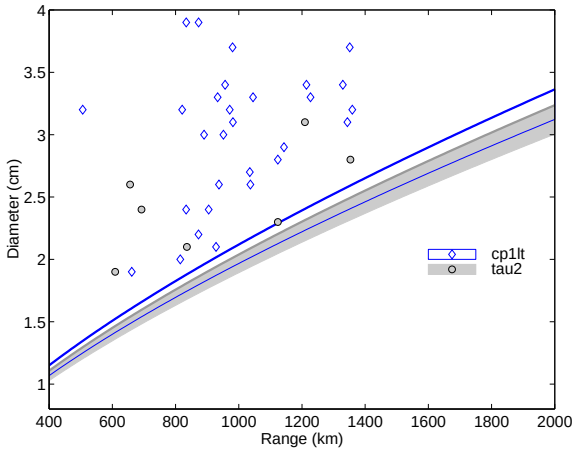

Figure 8: EISCAT UHF detection sensitivity limit with 0.3 s integration and 1 MW transmission power. The minimum detectable size is shown as function of range. There are two curves for both experiments used in the test campaign. The upper curve corresponds to the detection threshold $\mathcal{R}_{\max} = 5$ which we actually used in the test campaign, the lower curve corresponds to $\mathcal{R}_{\max} = 4$. The markers show effective diameters measured in the test campaign.

integration time is 0.3 s for both experiments. The assumed transmission power is 1 MW, which was typical during the test campaign. The sensitivity estimate in Fig. 8 also assumes that the coherent integration has been successful and that the GMF method estimates the peak signal amplitude correctly. In practice, several factors cause the signal amplitude to be underestimated, up to several tens of per cent. This reduces the actual sensitivity. On the other hand, the assumed transmission power in Fig. 8 is only half of the 2 MW that the refurbished EISCAT UHF transmitter is ultimately expected to deliver. Therefore, the curves in Fig. 8 should give a fair estimate of the detection sensitivity that can be achieved with the UHF system.

Figure 8 shows the small-diameter events from the test campaign. The full effective-size distribution is plotted in the top panel of Fig. 9. Because we do not usually know how far off-axis the target passed through the radar beam, its effective diameter gives only a lower bound for the actual size. One probably should not make strong inferences from a data set this small, but in the higher ranges, the events appear to lie rather far from the threshold curve. Range-integrated size distribution, containing all the analysed events, is shown in Fig. 10. Also it shows some kind of deficiency of events near the detection threshold. This might indicate that we do not detect all events that are near the detection threshold. Such an effect is to be expected, but a proper statistical study should be done about how large the effect should be.

Velocity and acceleration estimates

The remaining basic parameters, the Doppler-velocity and the acceleration, are shown in the middle and bottom panels of Fig. 9.

4.3 Comparison with a catalogued object

The strongest of the high-altitude tau2 events during the test campaign began at 22:19:06, 20 February 2001. The event was studied by M Landgraf from ESOC [8]. He identified the target as a large catalogued object, COSPAR ID 1994-11G. According to Landgraf, the object has total mass 1390 kg and cylindrical shape, with diameter 2.7 m and height 2.2 m. It has radar cross section 8.3 m^2. The target should have passed the EISCAT beam at the off-axis distance of 1.27°. Figure 11 shows our analysis summary plot of the event. The analysis was done with FastGMF, using 0.27 s integration.

The top panel of Fig. 11 shows the ratio $\mathcal{R}_{\max}$ during the beam transit. The antenna sidelobe structure is clearly visible. Markers indicate those scans where $\mathcal{R}_{\max}$ was larger than the threshold 4.5. To find the off-centre distance of the transit, we fitted the (theoretical) EISCAT antenna pattern to the $\mathcal{R}_{\max}$ data. The best fit was achieved by assuming that the transit

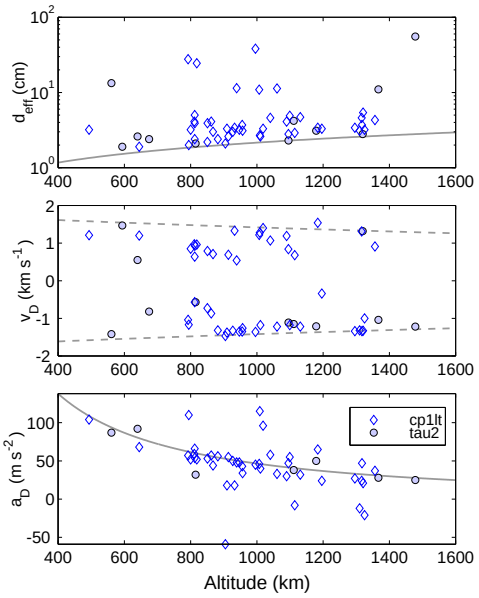

Figure 9: Parameter estimates in the test campaign. The data was analysed with the full GMF, with 0.3 s integration. The top panel shows the effective diameter, the solid line indicates the threshold diameter. The middle panel shows the Doppler-velocity v_{D}. The two dashed lines give the maximum and minimum radial velocity for targets in circular orbits, for the beam elevation 77°. The bottom panel shows the acceleration estimate, computed by a linear fit to v_{D} during the beam passage. The solid line is the vertical-beam, circular-orbit acceleration.

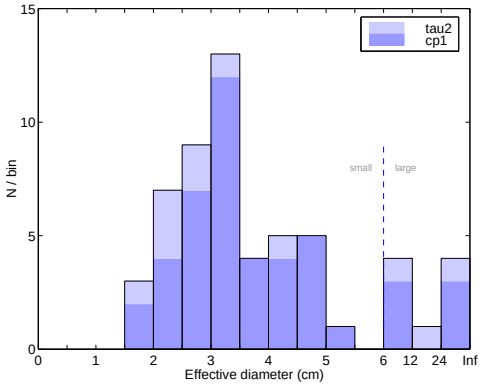

Figure 10: Size distribution of events in the test campaign. The dashed vertical line indicates the value $d_{\mathrm{eff}} \approx \lambda_{\mathrm{radar}}/5$, the figure's x-axis is non-linear to the right of this point.

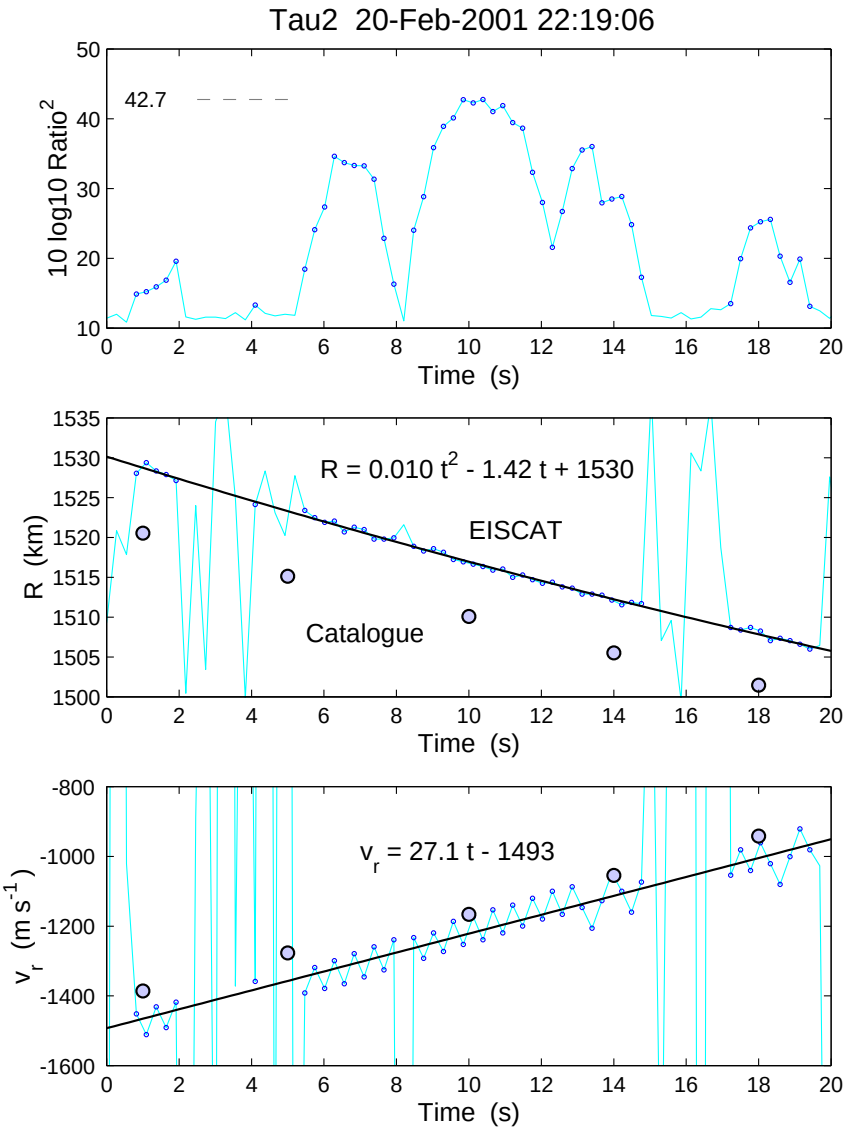

Figure 11: Event at 22:19:06, 20 February 2001, catalogue comparison. The top panel shows $\mathcal{R}_{\max}$ in dB. The middle panel shows the measured range (small circles), a parabolic fit, and the catalogue prediction (large circles). The bottom panel shows the measured Doppler-velocity (small circles), a linear fit, and the catalogue prediction for the range rate (large circles). The measurement was analysed with the FastGMF algorithm.

occurred 0.52° off-axis. It seems difficult to reconcile the predicted offset 1.27° with the inferred value 0.52°.

Panels (2) and (3) of Fig. 11 show the measured range and Doppler-velocity. The solid dark curves represent quadratic and linear fits to the good points. The large dots represent the predicted values. The measured range is about 7 km larger than predicted. The slope of the velocity curve is as predicted, but there is a discrepancy of about 0.1 km s^{-1} in the actual velocity values. The circular-orbit, vertical-beam acceleration is 27.5 m s^{-2}, which is consistent with the value 27.1 m s^{-2} from the velocity fit. According to Landgraf, the timing accuracy for the catalogued objects is of the order of 10 s, while we believe our timing to be accurate to within about 0.1 s. However, the range and velocity discrepancies cannot be removed simply by adjusting the relative timing, because the required correction would be about six seconds for the range data, but only about three seconds for the Doppler-data.

It is possible that the EISCAT pointing was not what we believed it was, azimuth 183.3° and elevation 77.1°. Normally, EISCAT pointing is known to be accurate to within 0.1°, but the February campaign took place after an exceptionally long maintenance and system upgrade period, after which no pointing calibration had yet been done.

5 Acknowledgements

We are indebted to Jyrki Rahkola of Invers Ltd for his work on the SD receiver, to Juha Pirttilä of Invers for providing the initial MEX implementation of the GMF algorithm, to Markku Markkanen of SGO for numerous clarifying discussions, and to the EISCAT staff for support during the test campaigns.

The EISCAT facility is supported by Finland (SA), France (CNRS), the Federal Republic of Germany (MPG), Japan (NIPR), Norway (NFR), Sweden (NFR), and the United Kingdom (PPARC).

References

[1] M. Baron *The EISCAT facility.* J. atmos. terr. Phys. 46, 469, 1984.

[2] M. Baron *EISCAT progress 1983–1985.* J. atmos. terr. Phys. 48, 767, 1986.

[3] G. Wannberg, I. Wolf, L.-G. Vanhainen, K. Koskenniemi, J. Röttger, M. Postila, J. Markkanen, R. Jacobsen, A. Stenberg, R. Larssen, S. Eliassen, S. Heck and A. Huuskonen *The EISCAT Svalbard radar: A case study in modern incoherent scatter radar system design.* Radio sci., 32, 2283, 1997.

[4] M. Lehtinen *Statistical theory of incoherent scatter radar measurements.* EISCAT Techn. Note 86/45, Eur. Incoherent Scatter Sci. Assoc., Kiruna, Sweden, 1986.

[5] M. I. Skolnik *Introduction to radar systems, second edition.* McGraw-Hill, Singapore, 1981.

[6] ESA Directorate of Technical and Operational Support ESOC Ground Segment Engineering Department Mission Analysis Section *Study specification, measurements of small-size debris with backscatter of radio waves.* Darmstadt, Germany,1999.

[7] J. Markkanen, M. Lehtinen, A. Huuskonen and A. Väänänen *Measurements of Small-Size Debris with Backscatter of Radio Waves. Final Report, ESOC Contract No. 13945/99/D/CD.* March 2002.

[8] M. Landgraf, Private communication, 2001.